SAND2022-3636C

Development and Characterization of a Tabletop Fog Chamber at Sandia National Laboratories

*Christian A. Patty[1], Jake Zenker[1], Elihu Deneke[1], Lekha Patel[1], Brian J. Redman[1], John D. van der Laan[1], Ryan L. Hastings[2], David W. Alexander[2], Kevin J. Webb[2], Andrew Glen[1], Andres L. Sanchez[1], Karl Westlake[1], Brian Z. Bentz[1], and Jeremy B. Wright[*1]*

[1]Sandia National Laboratories, P.O. Box 5800, Albuquerque, United States
[2]Purdue University, West Lafayette, IN 47907, United States
**jbwrigh@sandia.gov, fog@sandia.gov*

ABSTRACT

Atmospheric fog is a common degraded visual environment (DVE) that reduces sensing and imaging range and resolution in complex ways not fully encapsulated by traditional metrics. As such, better physical models are required to describe imaging systems in a fog environment. We have developed a tabletop fog chamber capable of creating repeatable fog-like environments for controlled experimentation of optical systems within this common DVE. We present measurement of transmission coefficients and droplet size distribution in a multiple scattering regime using this chamber.

Keywords: scattering, fog, degraded visual environment

1. INTRODUCTION

Fog is a naturally occurring atmospheric aerosol that scatters and absorbs light, causing a degraded visual environment (DVE)[1-7]. The DVEs caused by fog are often severe enough to impact optical imaging, detection, and ranging (e.g., LIDAR and LADAR), reducing situational awareness[2-4, 7, 8]. This decrease in situational awareness presents a problem for aviation, remote sensing, security, and many other systems which use optical signals to function[9, 10]. Fog is concerning because it can occur in most regions of the world, and with significant regularity in many areas[9, 10]. Furthermore, there is significant case-by-case variation between fogs in nature, even within the same region[9-11]. This creates a complex problem space, where optical systems must be able to function in a wide variety of scattering environments to be able to sense through fog. It is therefore important that we be able to repeatably generate multiple different fogs to test optical systems in a robust manner.

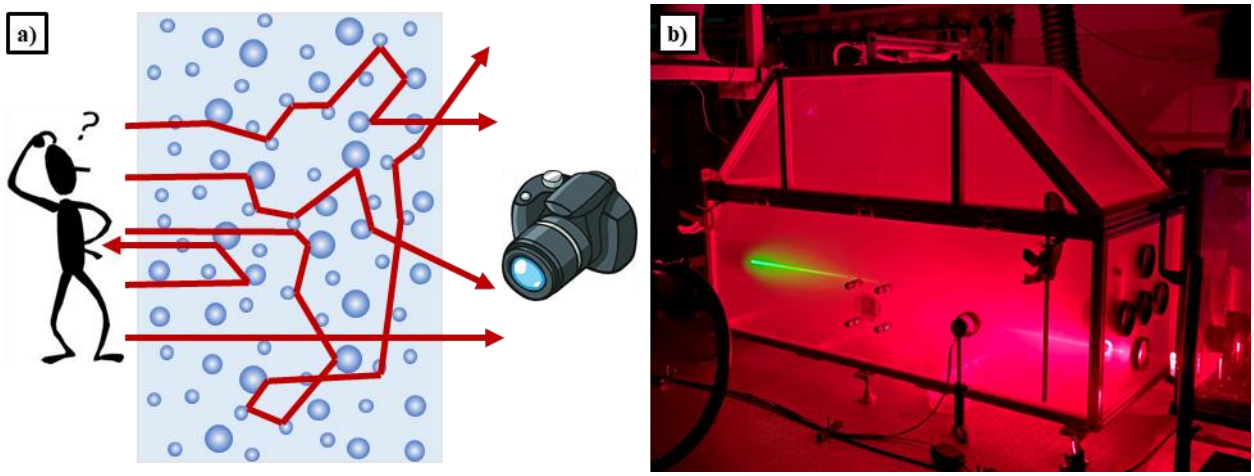

Figure 1: Scattering in fog, shown by **a)** a schematic depicting light randomly scattering as it passes through a fog and **b)** an image of light from two different collimated sources (a 670 nm red laser and a 532 nm green laser) being scattered in our tabletop fog chamber. Each beam travels about 30 cm before becoming isotropic.

Fog droplets degrade optical signals by randomly scattering and absorbing light[2-7], this affects both spatial resolution and intensity, causing blurring and loss of contrast[8]. This complex degradation makes resolving spatial features difficult, as many spatial information recovery techniques rely on contrast to distinguish features[2, 8]. Because signal is spatially scattered, intensity modelling metrics such as the Beer-Lambert Law fail to predict collimated light flux through fog. Thus, continued study and modelling are required to develop a robust, efficient solution that addresses signal degradation within fog. In our previous work we have utilized the Sandia National Laboratories Fog Chamber Facility (SNLFC) to generate replicable fog-like environments for testing[2-5, 7, 8]. Though this facility is well suited for large-scale testing in fog-like environments, the need for a small-scale system with rapid testing capabilities has become apparent. Such a system can provide a portable testbed for rapid experimentation with optical systems, allow for expedient characterization of generated fogs, and is described here.

The ability to test generation methods via our tabletop chamber will aid in the development of fog generation parameter sets to better simulate multiple real-world conditions for optical testing. In this paper we present relevant background and theory (**Section 2**), the design of our tabletop chamber (**Section 3**), our initial characterization experiments and the results (**Sections 4** and **5**), and a brief discussion of the applicability of our system (**Section 6**). We conclude with future work in **Section 7**.

2. BACKGROUND & THEORY

Naturally occurring fog is most often generated by either the rapid cooling of supersaturated air, or an atmospheric inversion of warm, moist air and cooler air[1, 5]. In either case, the thermodynamic equilibrium of fog droplet formation is described by the Köhler equation[1, 5]:

$$S_{v,w} = exp\left[\frac{2M_w\sigma_{s/r}}{RT\rho_w r} - \frac{v\phi_s m_s M_w/M_s}{(4\pi r^3\rho_s/3) - m_s}\right], \qquad \textbf{Equation 1}$$

where $S_{v,w}$ is the saturation ratio, M_w is the molecular weight of water, $\sigma_{s/r}$ is the droplet surface tension, R is the ideal gas law constant, T is the temperature, ρ_w is the density of water, r is the droplet radius, v is the number of dissolved ions, ϕ_s is the osmotic coefficient, m_s is the mass of solute, M_s is the molecular weight of the solute, and ρ_s is the density of the aqueous solution. For a given set of ambient conditions ($S_{v,w}$ and T are constant) droplet size is driven by the amount and type of solute present within a droplet[1, 5]. The droplet diameter can be changed by increasing or decreasing solute concentration.

Light scattering within fog can be approximated with Mie theory, wherein we calculate a scattering coefficient, a measure of the fog's ability to scatter light[1, 2, 4, 7]. A simplified calculation for the scattering coefficient (**Equation 2**) provides a useful basis for the discussions contained within this paper:

$$\mu_s = \frac{3V}{4\pi}\sum_i \frac{\sigma_{scatter}(r_i,\lambda)v_i}{r_i^3}, \qquad \textbf{Equation 2}$$

where μ_s is the scattering coefficient of the fog, V is the overall volume fraction of fog droplets in the air, $\sigma_{scatter}$ is the scattering cross section of a droplet with radius r_i for light with wavelength λ, and v_i is the relative volume fraction of droplets with radius r_i. This formulation is convenient because it shows the direct relationship between the scattering coefficient and overall droplet density and size distribution, which we can influence by adjusting the solute concentration within the droplets in accordance with **Equation 1**.

It is important we understand the fundamentals of **Equations 1** and **2** so that we can understand the effect that changing the solute concentration has on visibility. To do so we use the scattering Mean Free Path (MFP), l_s, which is the average distance between scattering events within the fog, given by:

$$l_s = \frac{1}{\mu_s}. \qquad \textbf{Equation 3}$$

This term is useful for understanding visibility as after ten (10) scattering events light from a collimated beam becomes isotropic, and information becomes challenging to decipher with conventional signal recovery approaches[2-4]. This term is also useful because we can use it to calculate the Meteorological Optical Range (MOR), which is defined as the distance required to reduce the flux of a collimated beam to 5% of its initial value. MOR is often used in transportation and

meteorology, and as such is a useful metric for comparing and communicating the impacts of different fogs[4, 8, 11]. We have shown before that in the visible spectrum, where water has low absorption, MOR can be approximated as the same distance as three (3) scattering paths[2, 12], giving:

$$MOR = \frac{-\ln(0.05)}{\mu_s} \approx 3l_s. \qquad \textbf{Equation 4}$$

This correlation both allows us to predict transmission through fog and provides a useful parameter for comparing our generated fogs to real-world atmospheric conditions, giving relevance to optical tests performed within our tabletop chamber.

3. TABLETOP CHAMBER DESIGN

Our final chamber design (**Figure 2a**) is a 48" x 18" x 15" rectangular chamber with an additional 15" of headspace to allow for fog generation and mixing. We designed the headspace as a 45° isosceles trapezoid to accommodate the angle of the spray nozzle while minimizing dead space above the rectangular testing chamber. The chamber is constructed from ¼" thick acrylic paneling and 1" aluminum t-slots, sealed with silicone epoxy at the connections and clamped along the lid line to ensure no leaks occur during experiments. The fog generation system consists of an air compressor, a water tank, and a 1/4J air atomizing spray nozzle from Spraying Systems Co. We selected this nozzle because it generates aerosolized droplets at atmospherically relevant diameters (<100 μm)[9]. The nozzle operates by atomizing a water flow from the tank with a shearing air flow, spraying fog droplets into the chamber. Both head pressure for the water tank and the shearing airflow are generated by the compressor.

The chamber is equipped with six optical paths (five across the long axis of the chamber and one across the short axis) each fitted with hydrophobic, optical windows which are transparent in the visible waveband, and multiple ports with Swage connections. These paths and ports allow for many different configurations of equipment to support testing needs. **Figure 2b** shows one such possible configuration of the test chamber, where several of the longer optical paths are utilized for fog characterization tests.

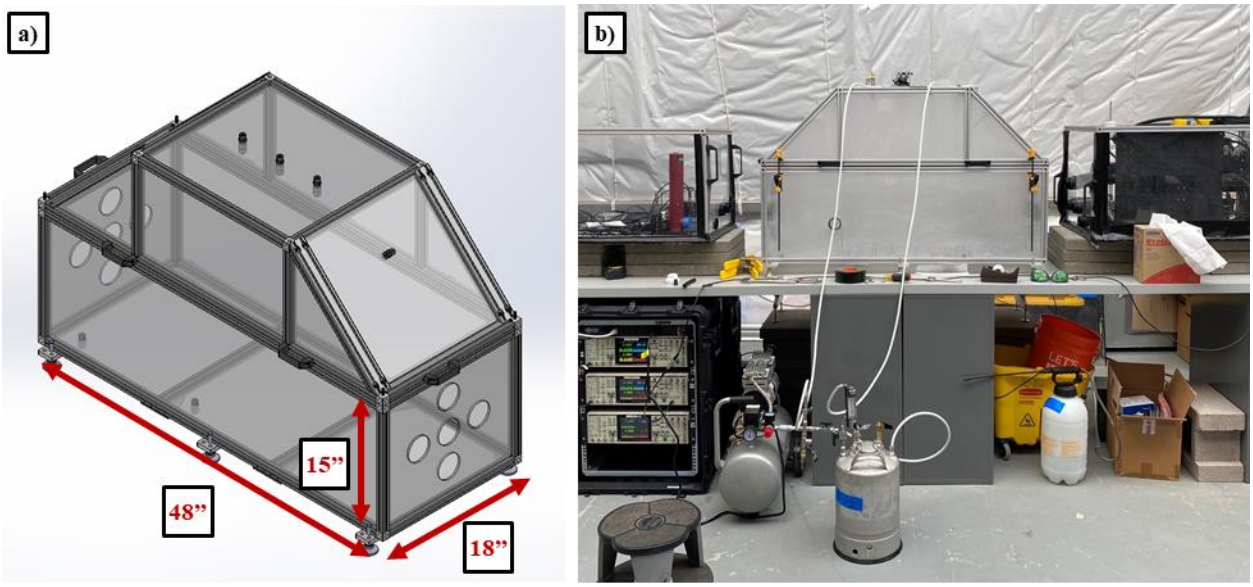

Figure 2: The Sandia National Laboratories Tabletop Fog Chamber shown both **a)** as an initial schematic and **b)** assembled at a test site.

4. FOG CHARACTERIZATION

4.1 Characterization Equipment

Droplet size distribution measurements were performed by a Malvern Spraytec, a diffraction-based particle sizer that was connected to the chamber via an inhalation cell. Optical transmission through the chamber was measured by a custom transmissometer built in house. This transmissometer measures transmission at multiple wavelengths (532 nm, 1,550 nm, and 9.68 μm), and can be aligned through the central full-length optical paths of the tabletop fog chamber, as shown in **Figure 2b**. We also measured relative humidity (RH), temperature, and barometric pressure inside and outside of the chamber with a pair of Omega RMYL loggers. All these pieces of equipment are also utilized at the SNLFC.

4.2 Spray Regime

We generate fog in the tabletop fog chamber by spraying through the nozzles until a maximum density is achieved, indicated by the stabilization of optical transmission through the chamber. We then turn off the fog generation system and allow the fog to dissipate. In the current configuration it takes the system three minutes to reach a maximum density and about ten minutes to dissipate, depending on the type of fog generated. Due to the low relative humidity (RH) at our test sites (an annual average of <40% RH) the humidity within the chamber must be increased prior to testing so the fog remains stable and is not lost humidifying the chamber. To accomplish this, we pretreat the chamber prior to each experimental run by first performing a "humidification spray'', a 15-minute-long spray of distilled water through the system which raises the RH within the chamber to saturation. Due to the Malvern inhalation cell causing significant humidity loss throughout experiments, we discovered that we were limited to five sprays per experiment before seeing a steep drop in RH, requiring re-humidification.

4.3 Fog Parameter Sets

It is essential to provide a testbed that can generate a wide range of fog-like environments for robust optical testing because of the significant variability seen in fogs formed in nature[9, 11]. To this end, we investigated the effect of adding a solute to the feed water of our fog generation system. In accordance with Köhler theory, and assuming similar atmospheric pressure and temperature between tests, we expected adding a solute would increase the mean droplet size and number of droplets in the generated fogs, thereby producing distinct test environments as a function of solute concentration. Over multiple experiments we generated fogs with both no solute (Tabletop Fog #1) and fogs with 10 g/L of salt (sodium chloride, NaCl) in the feed water (Tabletop Fog #2), holding all other parameters constant. Both parameter sets were run in triplicate, with each run consisting of five individual sprays, as discussed in **Section 4.2**, creating 15 fogs per parameter set for statistical analysis.

5. RESULTS

5.1 Tabletop Fog #1 (no solute in feed water)

The fog generated when no solute was present in the feed water had a maximum density of 1.6×10^5 droplets per cubic centimeter, with a mean droplet diameter of 1.58 μm (with standard deviation (SD) equal to 0.03 μm), a scattering MFP of $l_s = 0.4$ m, and a MOR of 1.1 m. Visual observation of this fog showed partial obscuration through the 18" short path length across the width of the chamber (**Figure 3a**). The droplet size distribution and count are consistent between individual sprays (**Figure 3b**), and across multiple tests.

5.2 Tabletop Fog #2 (10 g/L salt in feed water)

The fog generated with a 10 g/L salt concentration in the feed water had a maximum density of 4.2×10^6 droplets per cubic centimeter, a scattering MFP of $l_s = 0.16$ m, and a MOR of 0.49 m. Visual observation of this fog along the 18" short path length showed complete obscuration (**Figure 4a**). Like Tabletop Fog #1, the droplet size distribution and count are consistent between individual sprays (**Figure 4b**) and across multiple tests. Unlike Tabletop Fog #1 this fog had a bimodal distribution of droplet diameters. The primary mode had a mean droplet diameter of 1.73 μm (SD = 0.13 μm) while the secondary mode had a mean droplet diameter of 12.1 μm (SD = 0.09 μm). A direct comparison of Tabletop Fogs #1 and #2 can be seen in **Table 1**.

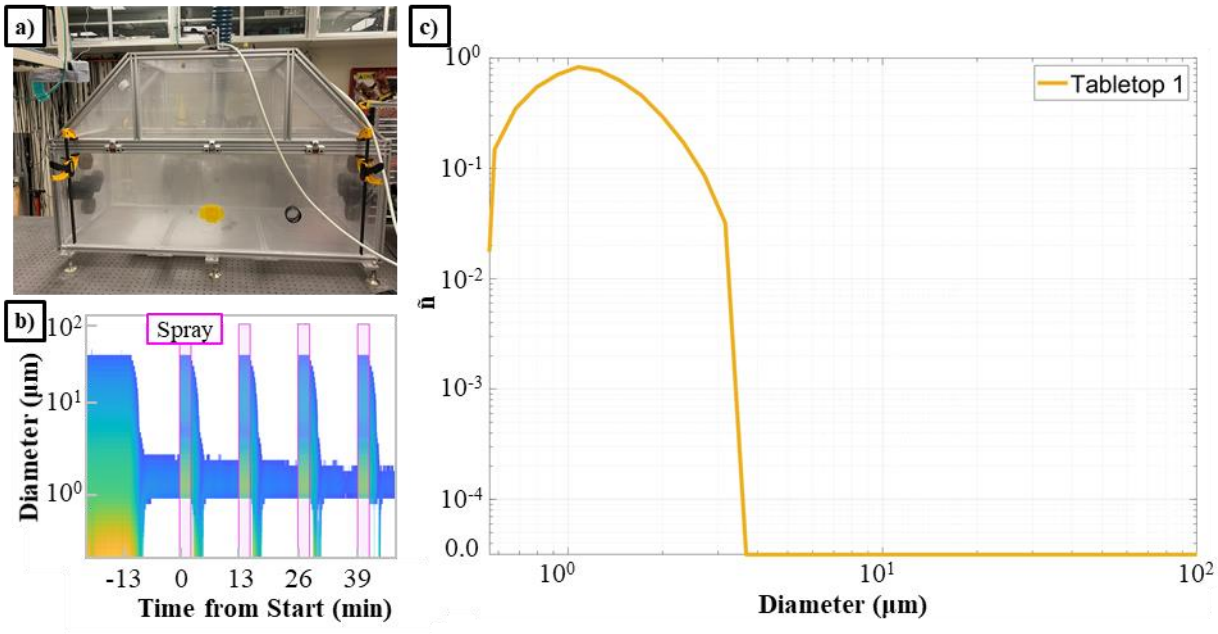

Figure 3: Tabletop Fog #1 test images and data, **a)** image of the chamber following a spray, when the fog is at its highest density, **b)** droplet size distribution heat map over multiple sprays, where pink boxes indicate a spray. Droplet size distributions are similar between sprays. **c)** Sampled Droplet size distribution of the fog at time = 8 minutes.

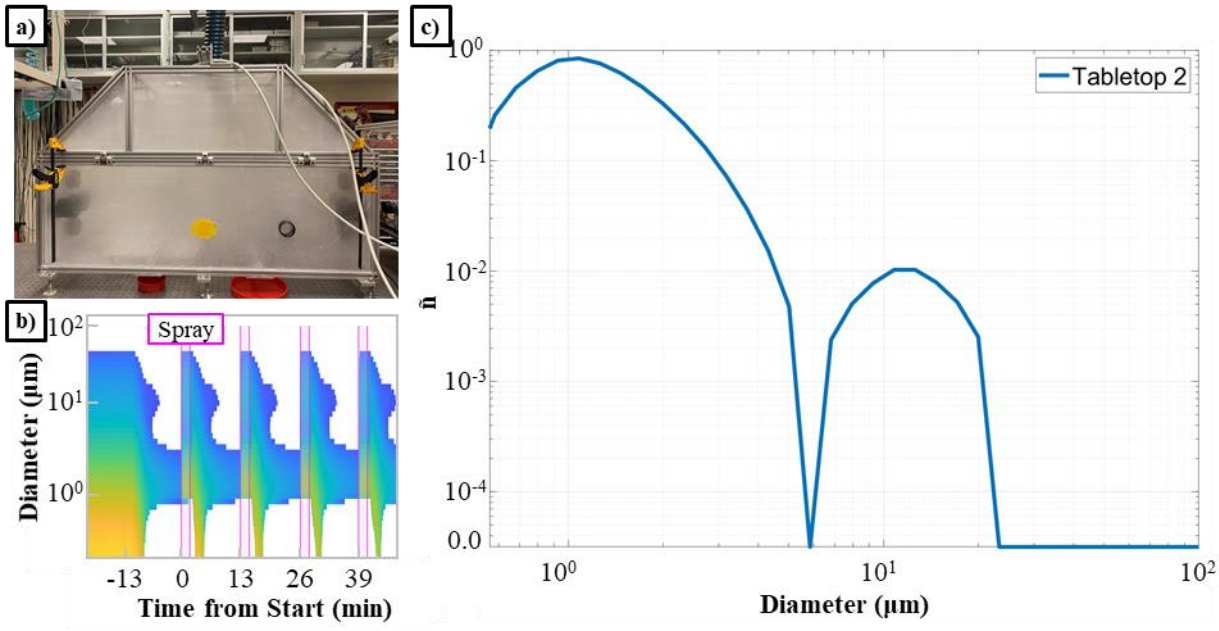

Figure 4: Tabletop Fog #2 test images and data, **a)** image of the chamber following a spray, when the fog is at its highest density, **b)** droplet size distribution heat map over multiple sprays, where pink boxes indicate a spray. Droplet size distributions are similar between sprays. **c)** Sampled Droplet size distribution of the fog at time = 8 minutes.

Table 1: Comparison of Tabletop Chamber Fogs to SNLFC and Real-World Fogs					
Fog Parameter Set	**Mean Diameter (μm) and standard deviation (SD)**	**Density (#/cm^3)**		**Mie Scattering Coefficient (m^{-1})**	**Average MOR (m)**
		Average	**Maximum**		
Tabletop #1 (no solute)	1.58; *SD = 0.03*	9.8 x 10^4	1.6 x 10^5	2.8	1.1
Tabletop #2 (10 g/L salt)	1.73; *SD = 0.13* 12.1; *SD = 0.09*	2.0 x 10^5	4.2 x 10^6	6.1	0.49
SNLFC (10 g/L salt)	2.21; *SD = 0.07* 39.9; *SD = 1.89*	1.5 x 10^5	2.2 x 10^5	1.0	3.0
Garland	1.15; *SD = 0.002*	3.2 x 10^3		---	290*

*observed at test site[11]

6. DISCUSSION & APPLICATIONS

By increasing the solute concentration in the feed water, we see a significant difference in the droplet diameter distribution, the average and maximum droplet density, and the average MOR of the generated fogs (**Table 1**). Both mean droplet diameter and density increase between Tabletop Fog #1 and #2, in turn reducing the average MOR of Tabletop Fog #2 by 50% when compared to Tabletop Fog #1. This effect can be seen by comparing the photos in **Figures 3a** and **4a**. This decrease is in good agreement with Köhler and Mie theory, which together predict a decrease in visibility as solute concentration increases. Though not discussed in **Section 2**, Köhler theory also predicts the presence of a bimodal diameter distribution, as seen in Tabletop Fog #2 (**Figure 4c**). To understand this, we refer to **Figure 5**, which depicts a Köhler curve for a hypothetical fog[1]. Köhler theory predicts droplet evolution will trend towards a local saddle point (point **B**, in **Figure 5**) where evaporation and condensation are balanced, or to grow past the critical diameter (indicated by the right edge of the grey bar in **Figure 5**) through mechanical collision, becoming "activated"[1]. An activated droplet will continue to absorb available humidity unless it loses sufficient water (through collisions) to shrink back below the critical diameter[1].

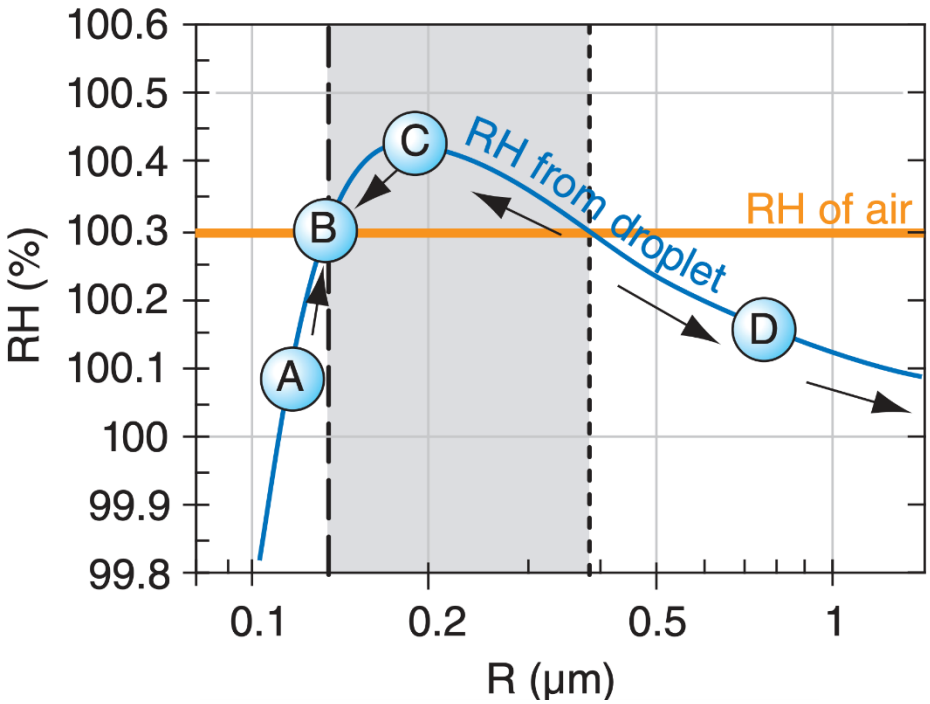

Figure 5: Graphical depiction of a Köhler curve, reproduced from Stull[1]. Droplets will tend to either grow or shrink towards saddle point **B**, or, if activated (surpassing the right side of the grey bar), increase until they are removed from the system by mechanical processes.

If this does not occur the droplet will either deposit along the chamber walls or precipitate out of the system via gravity[1]. In our tabletop chamber, the presence of a second mode shows that the system can be described by Köhler theory, and that the system can generate aerosols representative of observed atmospheric aerosols[1, 9, 11].

We have shown that our tabletop chamber can generate repeatable fogs when using the same parameter sets. This can be seen in both **Figures 3b** and **4b**, where droplet size distribution heat maps demonstrate high similarity between sprays, and in **Table 1**, where the standard deviation of droplet distributions are all less than 10% of the mean diameter. This level of repeatability is desirable when using this system as a testbed, as it allows for the repeated generation of the same conditions for testing.

We have also compared our tabletop chamber to the SNLFC, our large-scale research facility. **Figure 6** shows droplet size distributions of the fogs generated in the tabletop chamber plotted with fog measured in previous experiments at the SNLFC[2]. The SNLFC fog was generated in a manner like Tabletop Fog #2 in this experiment, with 10 g/L salt added to the feed water[2, 5, 6]. As is clear in **Figure 6**, both the SNLFC fog and Tabletop Fog #2 show a similar bimodal behavior due to the effect of the salt on droplet formation in a stable environment. This type of bimodal fog is referred to as an advection fog and is most often seen in coastal regions[5, 9, 11]. Replicating this type of fog has immediate application to testing optical systems intended for deployment in coastal regions, at sea, and in other areas where the dominant fog is advective in nature.

Figure 6 also includes the droplet size distribution of a historical real-world fog from Garland, *et al.*[11], labelled as "Garland". This fog has a tight unimodal distribution very similar to that seen in Tabletop Fog #1 from this experiment. This type of diameter distribution classifies these fogs as radiation fogs, which are more common inland, where there is less available humidity[5, 9-11]. Radiation fogs are often less dense than advection fogs, which we can also see if the case

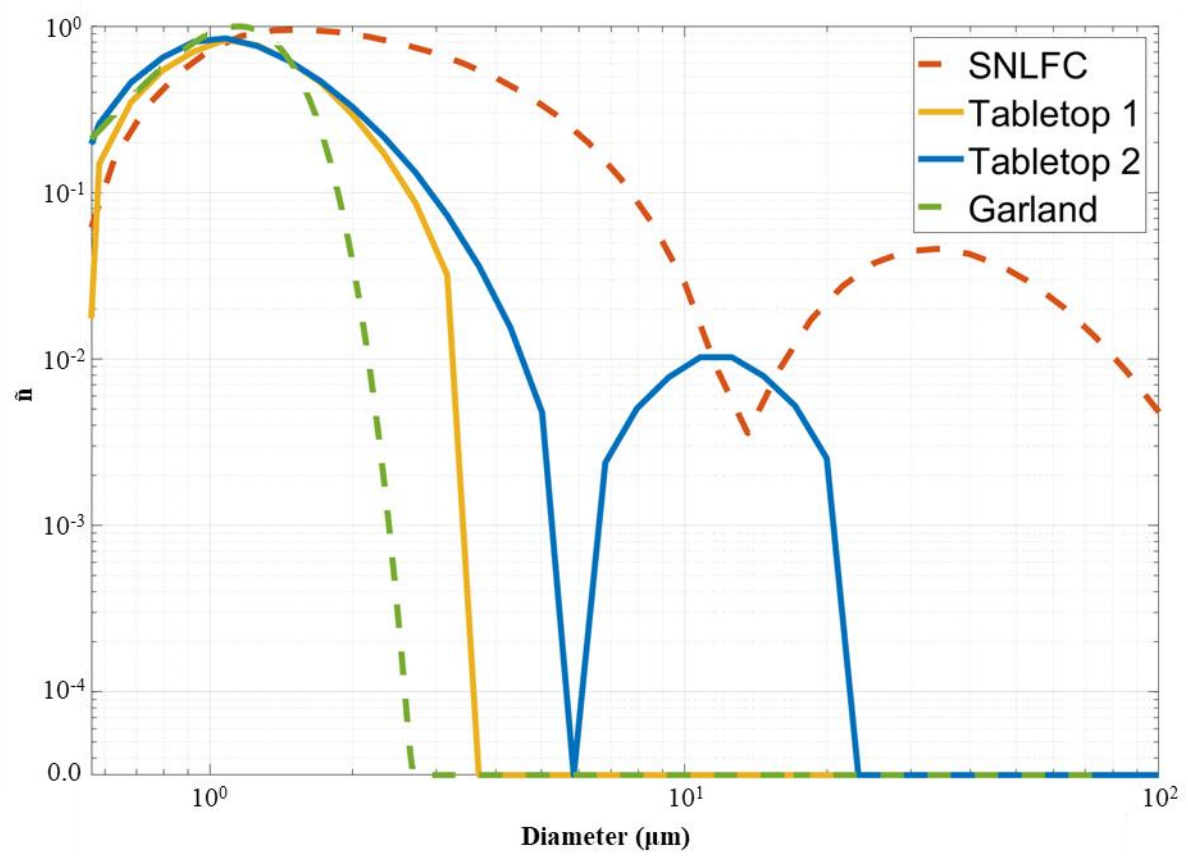

Figure 6: Comparison of droplet size distributions of fog measured in previous work at the SNLFC (SNLFC, from Bentz, *et al.*[2]), the fogs generated in our tabletop fog chamber (Tabletop 1 & 2, from this experiment), and historical real-world fog data (Garland, from Garland, *et al.*[11]).

when we compare Tabletop Fogs #1 and #2 in **Table 1**. There is also immediate relevance to being able to replicate radiative fogs for optical testing of systems that are intended to be deployed at inland facilities. Furthermore, the ability to replicate not just one, but multiple categories of fog is relevant to optical systems that might experience both radiation and advection fogs, such as those present on airplanes and in autonomous vehicles.

Furthermore, we can use the information present in **Figure 6** to compare the two chambers. This information is useful for informing experiments that wish to scale up or down between the two chambers, where being able to replicate conditions in each chamber will be essential to continuity of testing. By comparing the SNLFC fog to the Tabletop Fog #2 we can discern that the SNLFC facility maintains a higher RH than the tabletop chamber was able to during these experiments. This can be concluded by observing the larger mean droplet sizes of both modes in the SNLFC fog versus Tabletop Fog #2 and searching a Köhler curve (like the one presented in **Figure 5**) for the appropriate supersaturation point. This can also be concluded by solving **Equation 1** as given. The overall similarity between the SNLFC fog and Tabletop Fog #2 implies that we can expect our experiments in the tabletop chamber to scale well to the SNLFC, however we will need to secure better control over the RH and temperature conditions of the tabletop chamber to refine this process.

7. CONCLUSIONS & FUTURE WORK

Here we have discussed the design, initial testing, and applicability of a tabletop fog chamber. We have shown that this tabletop system has significant potential for use as an optics testbed for fog. We attribute this to the chamber's ability to generate several different fogs with a high level of repeatability, as we have shown in this paper.

Future work will continue to explore the impact of Köhler variables on fog generation with the goal of being able to create other types of fog with varying, real-world relevant densities and droplet size distributions. To that end, we intend to test different solute concentrations and injection methods and to develop better environmental control over the chamber. We will also continue to further refine these parameter sets to achieve consistent fog optical properties across multiple tabletop chambers, enabling others to build replicate chambers and generate the same fogs. This work is already underway, see **Figure 7**, in which a twin tabletop chamber at Purdue University is shown generating Tabletop Fog #2, using the parameters described in this paper. This work will also focus on optical testing, and we intend to use these twin chambers to explore sensing with speckle through fog, with the twin chamber depicted in **Figure 7** being used to run these experiments. We further intend to study the functionality of event-based detectors in fog environments and to study the evolution of angular scattering within fog using angle-space lenses.

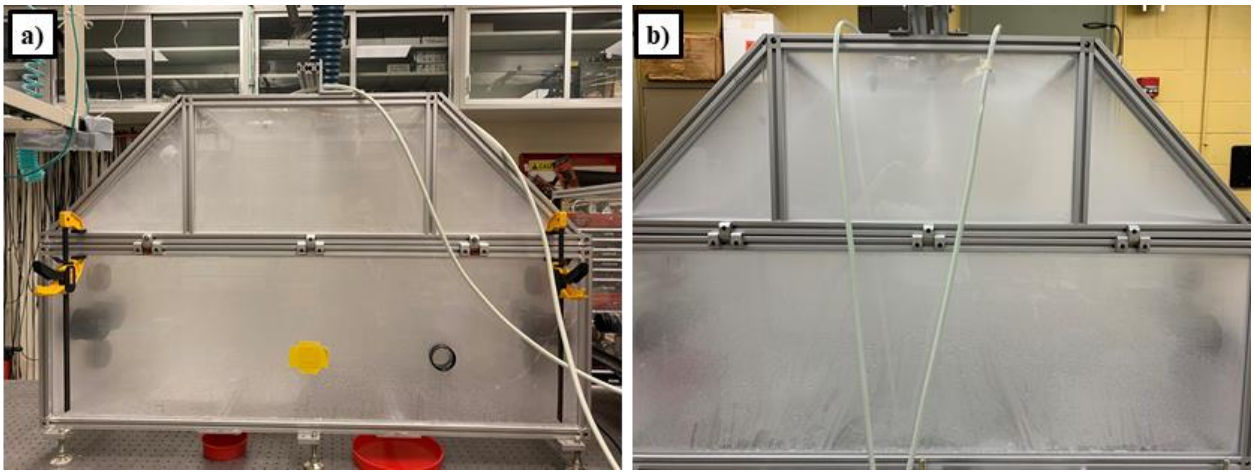

Figure 7: Photographs of our twin tabletop chambers generating the same fog, Tabletop Fog #2 from this experiment. The chamber depicted in **a)** is at our Sandia site in Albuquerque, NM, while the chamber depicted in **b)** is at Purdue University in West Lafyette, IN. On visual inspection the chambers generate a similar fog when using the same parameter set.

ACKNOWLEDGEMENTS

We would like to acknowledge and thank Matthew Tezak, Steven Storch, and Laura Lemieux for their work and contributions to the construction of this chamber.

This research was supported by the Laboratory Directed Research and Development (LDRD) Program at Sandia National Laboratories. This work was partially funded by NASA ARMD Transformational Tools and Technologies Project. Sandia National Laboratories is a multimission laboratory managed and operated by National Technology & Engineering Solutions of Sandia, LLC, a wholly owned subsidiary of Honeywell International Inc., for the U.S. Department of Energy's National Nuclear Security Administration under contract DE-NA0003525. This paper describes objective technical results and analysis. Any subjective views or opinions that might be expressed in the paper do not necessarily represent the views of the U.S. Department of Energy or the United States Government.

REFERENCES

[1] R. Stull, [Practical Meteorology] University of British Columbia, (2020).

[2] B. Z. Bentz, B. J. Redman, J. D. van der Laan, K. Westlake, A. Glen, A. L. Sanchez, and J. B. Wright, "Light transport with weak angular dependence in fog," Optics Express, 29(9), 13231-13245 (2021).

[3] B. Z. Bentz, C. A. Pattyn, J. D. van der Laan, B. J. Redman, A. Glen, A. L. Sanchez, K. Westlake, and J. B. Wright, "Incorporating the effects of objects in an approximate model of light transport in scattering media," Optics Letters, 47, (2022).

[4] B. Z. Bentz, J. D. van der Laan, A. Glen, C. A. Pattyn, B. J. Redman, A. L. Sanchez, K. Westlake, R. L. Hastings, K. J. Webb, and J. B. Wright, "Detection and localization of objects hidden in fog," Proceedings of SPIE 11759 (2021).

[5] J. B. Wright, J. D. v. d. Laan, A. Sanchez, S. A. Kemme, and D. A. Scrymgeour, "Optical characterization of the Sandia fog facility," Proceedings of SPIE 10197 (2017).

[6] J. D. van der Laan, J. B. Wright, S. A. Kemme, and D. A. Scrymgeour, "Superior signal persistence of circularly polarized light in polydisperse, real-world fog environments," Applied Optics, 57(19), 5464-5473 (2018).

[7] J. B. Wright, J. D. v. d. Laan, K. Westlake, B. Z. Bentz, A. L. Sanchez, A. Glen, and B. J. Redman, "Characterizing Fog at the Sandia Fog Facility," Proceedings of SPIE 11424 (2020).

[8] B. J. Redman, and J. D. van der Laan, "Measuring resolution degradation of long-wavelength infrared imagery in fog," Optical Engineering, 58(05), (2019).

[9] I. Gultepe, G. Pearson, J. A. Milbrandt, B. Hansen, S. Platnick, P. Taylor, M. Gordon, J. P. Oakley, and S. G. Cober, "The Fog Remote Sensing and Modeling Field Project," Bulletin of the American Meteorological Society, 90(3), 341-360 (2009).

[10] P. A. Pisano, L. C. Goodwin, and M. A. Rossetti, "US highway crashes in adverse road weather conditions," 24th conference on international interactive information and processing systems for meteorology, oceanography and hydrology (2008).

[11] J. A. Garland, "Some fog droplet size distributions obtained by an impaction method," Quarterly Journal of the Royal Meteorological Society, 97(414), 483-494 (1971).

[12] G. C. Birch, B. L. Woo, A. L. Sanchez, and H. Knapp, "Image quality, meteorological optical range, and fog particulate number evaluation using the Sandia National Laboratories fog chamber," Optical Engineering, 56(08), (2017).